Hard gluon emission from colored scalar pairs in e^+e^- annihilation

Ken-ichi Hikasa
Department of Physics, Tohoku University, Aoba-ku, Sendai 980-77, Japan

Junji Hisano
Department of Physics, Tokyo Institute of Technology, Oh-okayama, Meguro-ku, Tokyo 152, Japan
(Received 11 March 1996)

We study the QCD correction to the pair production of colored scalar particles in electron-position annihilation with an emphasis on gluon emission in the final state. We discuss the usefulness of working in a ''quasi-two-body'' frame and present the helicity amplitudes for the process. We compare the final-state configuration with fermion pair production and find that the three-jet fraction for the scalars shows quantitative differences from that for fermions. [S0556-2821(96)05815-8]

PACS number(s): 12.38.Bx, 12.60.Jv, 14.80.Ly

I. INTRODUCTION

The known elementary particles are either spin-1/2 fermions (quarks and leptons) or spin-1 gauge bosons. No elementary spin-0 particle has been found to date. Yet, scalar particles appear in most field theory models of particles. Higgs bosons are the key ingredient for electroweak symmetry breaking in the standard model and its extensions. Supersymmetry predicts a scalar partner for each fermion degree of freedom, thus, the existence of three generations of squarks and sleptons. The grand unified E_6 model contains colored scalar particles that may be interpreted either as leptoquarks or diquarks.

Many of these scalars can be pair produced in e^+e^- annihilation with a cross section comparable to or somewhat smaller than that for fermions. Experimental searches for these particles have been extensively performed [1].

If the scalar particle is colored (like the squark and leptoquark), the cross section is modified by QCD corrections. The calculation of the $O(\alpha_s)$ correction is essentially the same as the scalar QED one-loop calculation that has long been known.[1] The $O(\alpha_s)$ correction for the scalar pair production is numerically quite important. In the high energy limit, the total correction factor for scalar pair production is *four* times larger than that for fermion pair production [3]:

$$\sigma(e^+e^-\to\zeta\overline{\zeta}(g))=\sigma_0\left(1+3\frac{C_R\alpha_s}{\pi}\right), \tag{1.1}$$

where σ_0 is the lowest-order cross section and C_R is the second-order SU(3) Casimir eigenvalue (4/3 for the fundamental representation like squarks or leptoquarks). We use the notation ζ to represent a generic colored scalar particle in the representation R. At lower energies, especially in the threshold region, the correction factor becomes even larger.

The total $O(\alpha_s)$ correction consists of two parts, a one-loop virtual correction to the lowest-order process $e^+e^-\to\zeta\zeta$ and a real gluon emission correction $e^+e^-\to\zeta\overline{\zeta}g$, both of which are infrared divergent. This divergence is canceled when the two contributions are added. Essential for this cancellation is only the part of the three-body phase space where the gluon is soft (or collinear to one of the scalars when the scalar mass goes to zero). The rest of the three-body phase space corresponds to the final state with a hard gluon, which may be observed as a separate jet (''three-jet'' final state).

The gluon emission process in scalar top quark pair production has been studied by Beenakker, Höpker, and Zerwas [4], who calculated the fully differential cross section for $e^+e^-\to\tilde{t}\,\bar{\tilde{t}}g$. In the present paper, we derive the cross section in a different Lorentz frame (''quasi-two-body'' frame) in which the helicity amplitudes have a simple interpretation. We then extend their analysis and compare the three-jet cross sections with those for scalar and fermion pair production processes.

The QCD correction we calculate in this paper is just the effects arising from gluon gauge interactions. In the supersymmetric standard model there are additional interactions with the same strength involving gluinos. The gluino coupling contribution to the virtual $O(\alpha_s)$ correction is discussed by Arhrib, Capdequi-Peyranere, and Djouadi [5].

II. LOWEST-ORDER CROSS SECTION

We consider the process $e^+e^-\to\zeta\overline{\zeta}$ that occurs via s-channel γ or Z exchange. Additional t- or u-channel exchanges have to be included for selectron (or electron sneutrino) production or a leptoquark if it couples to electrons with a non-negligible Yukawa coupling.

In this section we list the lowest-order amplitude and cross section for completeness. The Feynman graph is shown in Fig. 1. The amplitude is found to be (see Fig. 1 for the momentum assignments)

$$\mathcal{M}_0=\frac{e^2}{s}H^\mu(p-\overline{p})_\mu, \tag{2.1}$$

with

[1] A detailed description can be found in Ref. [2]. A typographical error is corrected in Ref. [3].

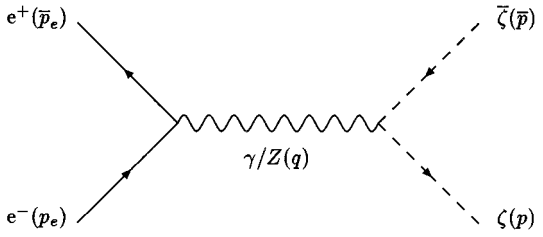

FIG. 1. Feynman diagram for $e^+e^-\to\zeta\overline{\zeta}$ at the lowest order.

$$H^\mu=-Q_\zeta\overline{v(p_e)}\,\gamma^\mu u(p_e)+\frac{T_{3\zeta}-Q_\zeta\sin^2\theta_W}{\cos^2\theta_W\sin^2\theta_W}\,\frac{s}{s-m_Z^2}\,\overline{v(p_e)}\,\gamma^\mu(v_e-a_e\gamma_5)u(p_e). \tag{2.2}$$

Here s is the e^+e^- c.m. energy squared, Q_ζ and $T_{3\zeta}$ are the electric charge and the third component of weak isospin of ζ, and

$$v_e=-\tfrac{1}{4}+\sin^2\theta_W,\quad a_e=-\tfrac{1}{4}. \tag{2.3}$$

We will neglect the electron mass throughout the paper.

For longitudinally polarized electrons with polarization P colliding with unpolarized positrons, the cross section can be written

$$d\sigma=\frac{1+P}{4}\,d\sigma_+ +\frac{1-P}{4}\,d\sigma_-, \tag{2.4}$$

where $d\sigma_\pm$ denotes the cross section for the $e_R^-e_L^+$ and $e_L^-e_R^+$ initial states. We find

$$\frac{d\sigma_\pm}{d\,\cos\theta}=\frac{\pi d_R\alpha^2\beta^3}{2s}\,H_\pm^2\sin^2\theta, \tag{2.5}$$

with

$$H_\pm=-Q_\zeta+\frac{(v_e\mp a_e)(T_{3\zeta}-Q_\zeta\sin^2\theta_W)}{\cos^2\theta_W\sin^2\theta_W}\,\frac{s}{s-m_Z^2}. \tag{2.6}$$

Here, d_R is the dimension of the color SU(3) representation of ζ (3 is for the fundamental representation), and

$$\beta=\sqrt{1-4m^2/s}, \tag{2.7}$$

with m being the ζ mass. The β^3 factor reflects the P-wave threshold. The total cross section is

$$\sigma_\pm=\frac{2\pi d_R\alpha^2\beta^3}{3s}\,H_\pm^2, \tag{2.8}$$

which we will denote by $\sigma_{0\pm}$.

III. $O(\alpha_s)$ CORRECTION

A. Virtual one-loop correction

Feynman diagrams for the process $e^+e^-\to\zeta\overline{\zeta}$ at $O(\alpha_s)$ are depicted in Fig. 2. The diagrams (a)–(c) are the one-particle-irreducible vertex corrections. The mixed four-point vertex in (b) and (c) appears because the scalar kinetic term has two covariant derivatives. The diagrams (d) and (e) are ζ self-energy corrections, and the diagrams (f)–(h) show the counterterm contribution.

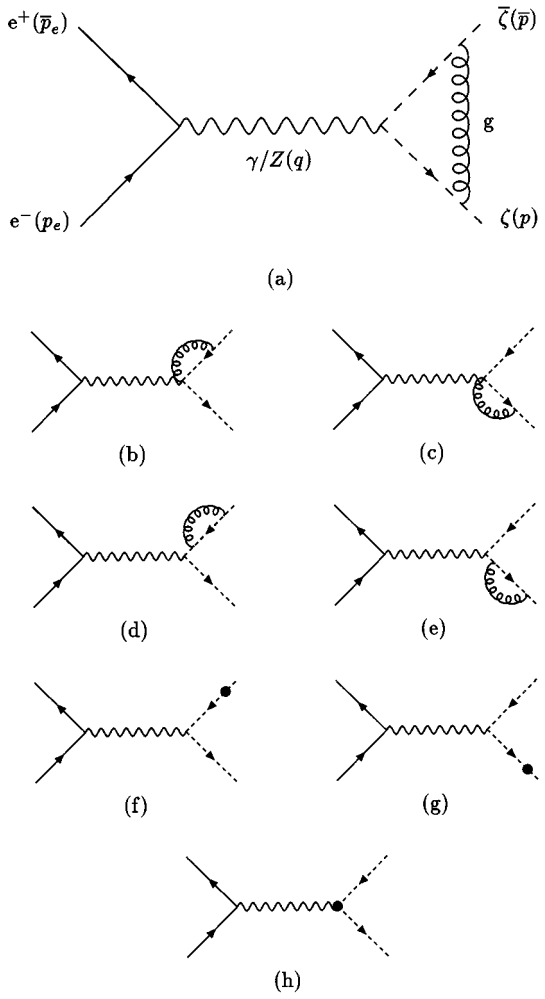

FIG. 2. Feynman diagrams for $e^+e^-\to\zeta\overline{\zeta}$ at $O(\alpha_s)$.

We regularize the ultraviolet divergence by dimensional reduction[2] with $D=4-2\epsilon$, and the infrared singularity by an infinitesimal gluon mass λ. This procedure does not cause problems with gauge invariance since the diagrams do not contain non-Abelian gauge vertices.

We adopt the on-shell renormalization scheme to determine the counterterms. The mass and wave function renormalization constants for ζ are found to be

$$\frac{\delta m^2}{m^2}=-\frac{C_R\alpha_s}{4\pi}\left[3\left(\frac{1}{\epsilon}-\gamma_E+\ln 4\pi\right)-3\ln\frac{m^2}{\mu^2}+7\right], \tag{3.1}$$

$$Z_\zeta-1=\frac{C_R\alpha_s}{4\pi}\left[2\left(\frac{1}{\epsilon}-\gamma_E+\ln 4\pi\right)-2\ln\frac{\lambda^2}{\mu^2}\right], \tag{3.2}$$

where μ is the renormalization scale and γ_E is the Euler constant.

[2]Naive dimensional regularization gives the same physical results, although the finite parts of the renormalization constants differ.

We write the $\zeta\bar{\zeta}\gamma$ vertex function in the form $-ieQ_\zeta\Lambda_\mu$ with

$$\Lambda_\mu = F(q^2)(p-\bar{p})_\mu . \tag{3.3}$$

(See Fig. 2 for the definition of the momenta.) Up to the order we work, the $\zeta\zeta Z$ vertex can be written as

$$\frac{-ie(T_{3\zeta}-Q_\zeta \sin^2\theta_W)}{\cos\theta_W \sin\theta_W}\,\Lambda_\mu \tag{3.4}$$

with the same Λ_μ. At the lowest order we have $F(q^2)=1$.

The counterterm for the vertex can be found using the Ward identity. The same result is obtained by requiring no $O(\alpha_s)$ correction at $q^2=0$, i.e., $F(0)=1$. Expanding the form factor as

$$F(q^2) = 1 + \frac{C_R\alpha_s}{2\pi} f(q^2), \tag{3.5}$$

we find, for $q^2 > 4m^2$,

$$\begin{aligned} f(q^2) = &\left(-\frac{1+\beta^2}{2\beta}\ln\frac{1+\beta}{1-\beta} + 1 \right)\ln\frac{m^2}{\lambda^2} \\ &+ \frac{1+\beta^2}{\beta}\left[\mathrm{Li}_2\left(\frac{1-\beta}{1+\beta}\right) - \ln\frac{2\beta}{1+\beta}\ln\frac{1+\beta}{1-\beta} \right. \\ &\left. - \tfrac{1}{4}\ln^2\frac{1+\beta}{1-\beta} + \frac{\pi^2}{3}\right] + \frac{1+\beta^2}{\beta}\ln\frac{1+\beta}{1-\beta} - 2 \\ &+ i\pi\,\frac{1+\beta^2}{2\beta}\left(\ln\frac{m^2}{\lambda^2} + \ln\frac{4\beta^2}{1-\beta^2} - 2 \right). \end{aligned} \tag{3.6}$$

Here $\mathrm{Li}_2(x)$ is the dilogarithm (Spence) function[3] $\mathrm{Li}_2(x) = -\int_0^x dt \ln(1-t)/t$. At $O(\alpha_s)$, the lowest-order cross section is multiplied by the factor

$$1 + \frac{C_R\alpha_s}{\pi}\,\mathrm{Re}\, f(s). \tag{3.7}$$

The infrared singularity is canceled by real gluon emission, to which we now turn.

B. Real gluon emission

The Feynman diagrams for the process $e^+e^- \to \zeta\bar{\zeta}g$ at the lowest order are shown in Fig. 3. The amplitudes are found to be

$$\mathcal{M} = \frac{e^2 g_s T^a}{s} H^\mu \left[\frac{(p-\bar{p}+k)_\mu p_\alpha}{p\cdot k} - \frac{(p-\bar{p}-k)_\mu \bar{p}_\alpha}{\bar{p}\cdot k} - 2g_{\mu\alpha} \right] \epsilon^{*\alpha}. \tag{3.8}$$

Here T^a is the SU(3) generator in the representation R.

We calculate the cross section for this process in two methods, with agreeing results. One is the conventional trace technique. The other method is a helicity amplitude technique described in Appendix A.

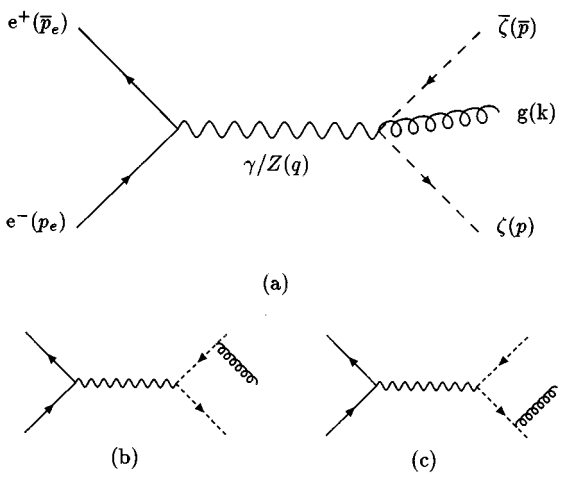

FIG. 3. Feynman diagrams for $e^+e^- \to \zeta\bar{\zeta}g$.

The differential cross section may be parametrized by four variables. We find it convenient to use the following four: τ, $\zeta\zeta$ c.m. energy squared normalized to s, $\tau = (p+\bar{p})^2/s$; Θ, angle between the e^- and the gluon in the e^+e^- c.m. frame; θ, angle between the ζ and the gluon in the $\zeta\zeta$ c.m. frame; ϕ azimuthal angle between the e^- and the ζ with respect to the gluon, measured from the e^- to the ζ direction (common to both frames).

The use of these variables is motivated by the fact that the amplitude can be split into two subprocesses $e^+e^- \to V^*(V^* = \gamma, Z)$ and $V^* \to \zeta\zeta g$, and the latter process can be most conveniently evaluated in the $\zeta\zeta$ c.m. frame. The detail and the result for the helicity amplitudes may be found in Appendix A.

The polarized cross section is

$$\begin{aligned} &\frac{d\sigma_\pm}{d\tau\, d\cos\Theta\, d\cos\theta\, d\phi} \\ &= \frac{d_R\alpha^2 H_\pm^2}{8s}\,\frac{C_R\alpha_s}{\pi}\, v(1-\tau)\{A(1+\cos^2\Theta) \\ &\quad + B(1-3\cos^2\Theta) + C\sin\Theta\cos\Theta\cos\phi \\ &\quad + D\sin^2\Theta\cos 2\phi\}, \end{aligned} \tag{3.9}$$

where

$$A = 1 + \frac{2\beta^2\tau v^2\sin^2\theta}{(1-\tau)^2(1-v^2\cos^2\theta)^2}, \tag{3.10a}$$

$$B = \frac{2\tau v^4\sin^2\theta\cos^2\theta}{(1-\tau)^2(1-v^2\cos^2\theta)^2}, \tag{3.10b}$$

$$C = -\frac{4\sqrt{\tau}v^2\sin\theta\cos\theta[\beta^2 - v^2 + (1+\tau)v^2\sin^2\theta]}{(1-\tau)^2(1-v^2\cos^2\theta)^2}, \tag{3.10c}$$

$$D = -\frac{2\tau v^2\sin^2\theta(\beta^2 - v^2\cos^2\theta)}{(1-\tau)^2(1-v^2\cos^2\theta)^2}. \tag{3.10d}$$

[3]For a convenient expansion for numerical evaluation of dilogarithm, see Ref. [6].

Here

$$v=\sqrt{1-4m^2/\tau s} \tag{3.11}$$

is the velocity of ζ in the $\zeta\bar{\zeta}$ c.m. frame.

If one integrates the cross section over the whole three-body phase space, one encounters infrared divergence coming from the soft-gluon region. We separate this region from the rest by the condition that the gluon energy $k^0<\omega$, where the cutoff ω is infinitesimally small.

In this region, we regularize the divergence by giving an infinitesimal mass λ to the gluon, which satisfies $\lambda\ll\omega$. We recalculate the amplitude with finite mass. The amplitude factorizes into the lowest-order part and the soft gluon factor. Since a very soft gluon does not alter the kinematics of the $\zeta\zeta$ state, we can also integrate over the soft-gluon phase space ignoring momentum conservation. Integrating over this soft-gluon region, we find the cross section

$$\begin{aligned}\sigma_{\rm soft}=\sigma_0\,\frac{C_R\alpha_s}{\pi}\Bigg\{&\left(\frac{1+\beta^2}{2\beta}\ln\frac{1+\beta}{1-\beta}-1\right)\ln\frac{4\omega^2}{\lambda^2}\\&+\frac{1+\beta^2}{\beta}\left[\mathrm{Li}_2\left(\frac{1-\beta}{1+\beta}\right)-\ln\frac{2\beta}{1+\beta}\ln\frac{1+\beta}{1-\beta}\right.\\&\left.-\tfrac{1}{4}\ln^2\frac{1+\beta}{1-\beta}-\frac{\pi^2}{6}\right]+\frac{1}{\beta}\ln\frac{1+\beta}{1-\beta}\Bigg\},\end{aligned} \tag{3.12}$$

where σ_0 is the lowest-order cross section.

For the rest of the phase space, we can set the gluon mass to zero. We first integrate over Θ,ϕ to find

$$\begin{aligned}\frac{d\sigma_\pm}{d\tau\,d\cos\theta}=\sigma_{0\pm}\,\frac{C_R\alpha_s}{\pi}\,\frac{v(1-\tau)}{\beta^3}\\\times\left[1+\frac{2\beta^2\tau v^2\sin^2\theta}{(1-\tau)^2(1-v^2\cos^2\theta)^2}\right],\end{aligned} \tag{3.13}$$

which we will use to study the event configuration in the next section. The integrated cross section is

$$\begin{aligned}\sigma_{\rm hard}=\sigma_0\,\frac{C_R\alpha_s}{\pi}\Bigg\{&\left(\frac{1+\beta^2}{2\beta}\ln\frac{1+\beta}{1-\beta}-1\right)\ln\frac{m^2}{4\omega^2}\\&+\frac{1+\beta^2}{\beta}\left[2\,\mathrm{Li}_2\left(\frac{1-\beta}{1+\beta}\right)+2\,\mathrm{Li}_2\left(-\frac{1-\beta}{1+\beta}\right)\right.\\&\left.-\ln\frac{2}{1+\beta}\ln\frac{1+\beta}{1-\beta}+\tfrac{1}{2}\ln^2\frac{1+\beta}{1-\beta}-\frac{\pi^2}{6}\right]-3\ln\frac{4}{1-\beta^2}\\&-4\ln\beta-\frac{1}{4\beta^3}(3+\beta^2)(1-\beta^2)\ln\frac{1+\beta}{1-\beta}\\&+\frac{1}{2\beta^2}(3+7\beta^2)\Bigg\}.\end{aligned} \tag{3.14}$$

The ω dependence cancels out when these two cross sections are summed. The infrared divergence is canceled by adding the virtual one-loop correction discussed in the previous subsection.

C. Total correction

The $O(\alpha_s)$ corrected cross section for $e^+e^-\to\zeta\bar{\zeta}(g)$ can, thus, be written as

$$\sigma=\sigma_0\left[1+\frac{C_R\alpha_s}{\pi}\,\Delta\right], \tag{3.15}$$

where

$$\begin{aligned}\Delta=&\frac{1}{\beta}A(\beta)+\frac{1}{4\beta^3}(-3+10\beta^2+5\beta^4)\ln\frac{1+\beta}{1-\beta}\\&+\frac{3}{2\beta^2}(1+\beta^2),\end{aligned} \tag{3.16}$$

with

$$\begin{aligned}A(\beta)=(1+\beta^2)\Bigg[&4\,\mathrm{Li}_2\left(\frac{1-\beta}{1+\beta}\right)+2\,\mathrm{Li}_2\left(-\frac{1-\beta}{1+\beta}\right)\\&-3\ln\frac{2}{1+\beta}\ln\frac{1+\beta}{1-\beta}-2\ln\beta\ln\frac{1+\beta}{1-\beta}\Bigg]\\&-3\beta\ln\frac{4}{1-\beta^2}-4\beta\ln\beta.\end{aligned} \tag{3.17}$$

This may be compared with the corresponding formulas for the pair production of a colored fermion pair via vector and axial vector currents (the detail on the latter may be found in Appendix C):

$$\Delta_V=\frac{1}{\beta}A(\beta)+\frac{33+22\beta^2-7\beta^4}{8\beta(3-\beta^2)}\ln\frac{1+\beta}{1-\beta}+\frac{3(5-3\beta^2)}{4(3-\beta^2)}. \tag{3.18}$$

$$\begin{aligned}\Delta_A=&\frac{1}{\beta}A(\beta)+\frac{1}{32\beta^3}(21+59\beta^2+19\beta^4-3\beta^6)\ln\frac{1+\beta}{1-\beta}\\&+\frac{3}{16\beta^2}(-7+10\beta^2+\beta^4).\end{aligned} \tag{3.19}$$

The dependence on β of the cross section normalized to its lowest-order value is shown in Fig. 4. The corresponding quantities for fermion pair production are also shown for comparison. The correction for scalars is larger than that for fermions via vector current for all values of β. The correction for fermions via axial current is equal to that for vector current at the high-energy limit (which reflects the chiral symmetry in this limit), but approaches the scalar curve at small β. This latter behavior reflects the fact that spin does not play an important role in the nonrelativistic region. The difference of the vector current result is due to its S-wave dynamics in contrast with the P-wave behavior of the others.

At the high energy limit $\beta\to1$, one finds

$$\Delta=3,\quad \Delta_V=\Delta_A=\tfrac{3}{4}. \tag{3.20}$$

The correction for the scalar pair is four times larger. Near the threshold, one has

$$\Delta\simeq\Delta_A\simeq\frac{\pi^2}{2\beta}-2,\quad \Delta_V\simeq\frac{\pi^2}{2\beta}-4. \tag{3.21}$$

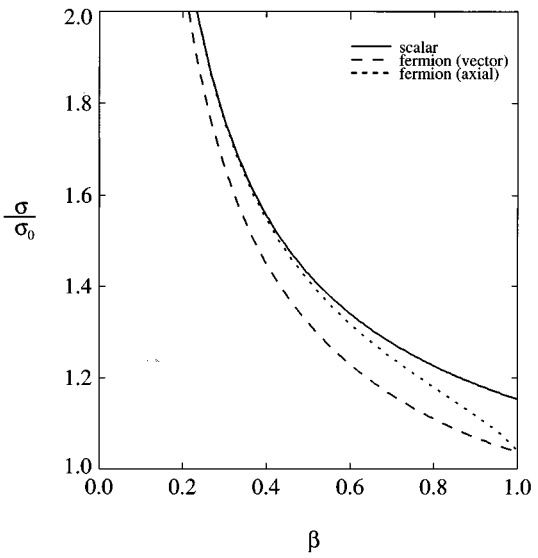

FIG. 4. Total $O(\alpha_s)$ correction to the pair production cross section of scalar pair (solid); fermion pair via vector current (dash); fermion pair via axial current (dotted). All curves are for particles in the fundamental color representation ($C_R=4/3$) and the strong coupling constant $\alpha_s=0.12$.

The terms proportional to $1/\beta$ are the consequence of Coulomb gluon exchange.

It is well known that perturbation expansion in α_s breaks down very near the threshold and one has to sum over ladder Coulomb gluon diagrams [2]. For the case of scalar pair production with the P-wave threshold behavior, the lowest-order cross section is proportional to β^3, which is modified to β^2 by the $O(\alpha_s)$ correction. The nonperturbative contribution further enhances the cross section and leads to a constant cross section at the threshold [7]. In the nonrelativistic approximation with the Coulomb potential (one gluon exchange approximation), the cross section is

$$\sigma_{\pm}=\frac{2\pi^2 d_R\alpha^2}{3s}H_{\pm}^2\frac{C_R\alpha_s(\beta^2+\frac{1}{4}C_R^2\alpha_s^2)}{[1-\exp(-\pi C_R\alpha_s/\beta)]}, \quad (3.22)$$

which gives at the threshold

$$\Delta=\frac{\pi^2 C_R^2\alpha_s^2}{4\beta^3}. \quad (3.23)$$

This effect becomes important only at very near threshold, $\beta\sim 0.1$, however.

If one approaches closer to the threshold, one will encounter P-wave $\zeta\zeta$ bound states, similar to charmonium and bottomonium resonances. These states are expected to be less pronounced than the fermion bound states, since the resonance formation cross section is proportional to the derivative of the wave function at the origin and is suppressed by a factor of α_s^2 compared to the fermion bound states. In the Coulomb potential approximation, this subthreshold cross section is given by [7]

$$\sigma_{\pm}=\frac{\pi^2 d_R\alpha^2}{12}H_{\pm}^2(C_R\alpha_s)^5\sum_{n=2}^{\infty}\frac{n^2-1}{n^5}\delta(s-M_n^2), \quad (3.24)$$

where $M_n=2m-C_R^2\alpha_s^2 m/4n^2$. This Coulombic approximation ignores the effect of confinement and is not adequate especially for higher bound states. One needs to solve the Schrödinger equation with a realistic color-force potential to obtain the cross section in the resonance region.

If ζ has a short lifetime with $\Gamma\gtrsim\alpha_s^2 m$, it does not live long enough to form a bound state. There will be only a smooth bump or shoulder instead of the resonances at the threshold. The situation will be similar to the case for the top quark pair production [8] and the cross section can be calculated quite reliably within perturbative QCD.

IV. JET CONFIGURATION

In this section we study the shape of the three-body final state $\zeta\zeta g$ when the gluon is ''visible.'' We compare various distributions with those for the more familiar final state of a fermion pair plus a gluon.

To define the final-state configuration, it is convenient to use Lorentz-invariant kinematic variables. We use the following Dalitz variables

$$x=\frac{2p\cdot k}{s}, \quad \overline{x}=\frac{2\overline{p}\cdot k}{s}, \quad (4.1)$$

for which the phase-space density is constant. The $\zeta\overline{\zeta}g$ cross section is (we drop the subscript $\pm$ from here on)

$$\frac{d\sigma}{dx\,d\overline{x}}=\sigma_0\frac{C_R\alpha_s}{\pi}\frac{1}{\beta}\left[\frac{2}{\beta^2}-\left(\frac{1}{x}+\frac{1}{\overline{x}}\right)+\frac{1+\beta^2}{2}\frac{1}{x\overline{x}}-\frac{1-\beta^2}{4}\left(\frac{1}{x^2}+\frac{1}{\overline{x}^2}\right)\right]. \quad (4.2)$$

The infrared singularity arises when the gluon energy is very small, $x\sim\overline{x}\sim 0$. At the high-energy limit, additional singularity arises from the region of the phase space in which the gluon momentum is parallel to that of ζ or $\overline{\zeta}$. This collinear region is characterized as $x\sim 0$ or $\overline{x}\sim 0$. In these singular regions, it is practically impossible to observe the existence of the extra gluon in the final hadron system. We therefore treat the $\zeta^{(-)}$ + gluon system as a $\zeta^{(-)}$ jet when the $\zeta^{(-)}g$ invariant mass is sufficiently close to the ζ mass.

We thus divide the three-body phase space into the two-jet and three-jet regions. The two-jet region is defined as

$$x<x_c \ \text{ or } \ \overline{x}<x_c \quad (4.3)$$

and the rest is the three-jet region. The two-jet cross section is the sum of the $\zeta\zeta$ cross section and the $\zeta\zeta g$ cross section in the two-jet region.

In the high-energy limit $\beta\to 1$, the integrated three-jet cross section is found to be

$$\sigma_{3j}/\sigma_0=\frac{C_R\alpha_s}{\pi}\left[2\mathrm{Li}_2(x_c)+\ln^2 x_c-\frac{\pi^2}{6}-2(1-x_c)\right.$$
$$\left.\times\ln\frac{1-x_c}{x_c}+(3-2x_c)(1-2x_c)\right], \tag{4.4}$$

whereas for fermions (both vector and axial) we have

$$\sigma_{3j}/\sigma_0=\frac{C_R\alpha_s}{\pi}\left[2\mathrm{Li}_2(x_c)+\ln^2 x_c-\frac{\pi^2}{6}\right.$$
$$\left.-\tfrac{1}{2}(1-x_c)(1-3x_c)\ln\frac{1-x_c}{x_c}+\tfrac{5}{4}(1-2x_c)\right]. \tag{4.5}$$

In Fig. 5, we show the three-jet fraction as a function of x_c. (Here and in the following figures, we plot σ_{3j} normalized to the $O(\alpha_s)$ total cross section, not to the lowest-order cross section.) The three-jet fraction for the scalar is larger than that for the fermion at large x_c but becomes smaller at small $x_c \lesssim 0.1$. The approximate form for small x_c is

$$\sigma_{3j}/\sigma_0 \simeq \frac{C_R\alpha_s}{\pi}\left[\ln^2 x_c+2\ln x_c+3-\frac{\pi^2}{6}\right] \tag{4.6}$$

for scalars, and

$$\sigma_{3j}/\sigma_0 \simeq \frac{C_R\alpha_s}{\pi}\left[\ln^2 x_c+\tfrac{3}{2}\ln x_c+\tfrac{5}{4}-\frac{\pi^2}{6}\right] \tag{4.7}$$

for fermions. These predictions are not reliable at very small x_c since higher-order contributions become important.

The three-jet fraction for finite m has a very complicated expression and we do not write down the analytic expression here. Instead, we show the numerical result for σ_{3j}/σ for several values of β in Fig. 6. For a fixed value of x_c, the three-jet fraction rapidly decreases as β becomes smaller. Hard gluon emission is greatly suppressed when one approaches the threshold. This suppression comes from the available phase space and from the structure of the gluon-emission vertex. The large QCD enhancement near the threshold can be attributed to the two-jet configuration and one can assume that most events in the threshold region have no extra jets in experimental searches for new colored scalar particles.

Toward the threshold region, the three-jet fraction in Fig. 6 for scalar pairs becomes similar to that for fermion pairs from the axial current. The fermion pair from the vector current shows a different behavior. This again reflects the fact that spin of the particle is not important in the nonrelativistic region.

In jet analyses in e^+e^- physics, one normally uses a jet-defining algorithm by combining momentum of hadrons and compares the result with the corresponding quantity in the quark-gluon system. A commonly adopted prescription uses the invariant mass of the hadron system to define a jet. To conform with this algorithm, we may use the invariant mass variables

$$y=\frac{(p+k)^2}{s}, \quad \overline{y}=\frac{(\overline{p}+k)^2}{s}, \tag{4.8}$$

instead of x and $\overline{x}$. These variables are related by

$$y=x+\frac{m^2}{s}, \quad \overline{y}=\overline{x}+\frac{m^2}{s}. \tag{4.9}$$

The definition of three-jet events in terms of y is

$$y>y_c \quad \text{and} \quad \overline{y}>y_c. \tag{4.10}$$

The three-jet fraction as a function of y_c is shown in Fig. 7.

So far we have assumed that we can somehow distinguish a ζ jet and a gluon jet. If this is not the case, we need to treat the three final particles in a democratic way and define the three-jet region as

$$y>y_c \quad \text{and} \quad \overline{y}>y_c \quad \text{and} \quad y_g>y_c, \tag{4.11}$$

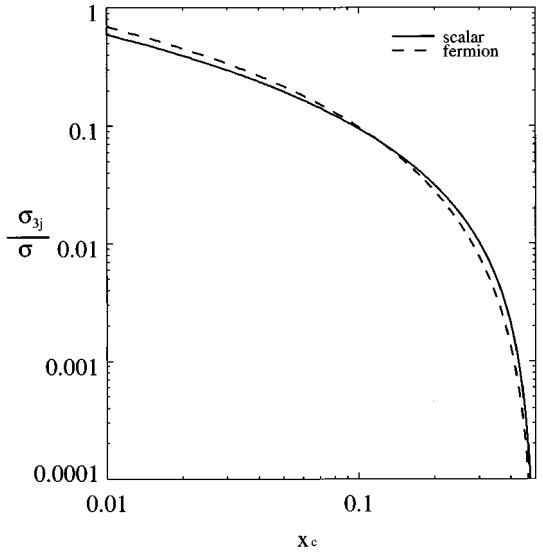

FIG. 5. Three-jet fraction for scalar (solid) and fermion (dashed) at the high-energy limit, for $\alpha_s=0.12$ and $C_R=4/3$.

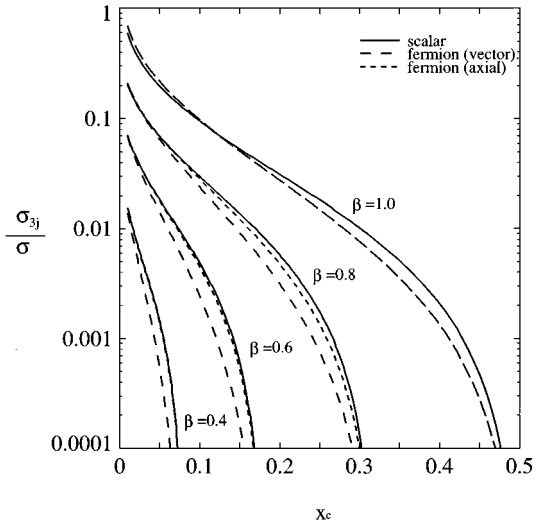

FIG. 6. Three-jet fraction for scalar (solid), fermion-vector (dashed), and fermion-axial (dotted) for $\beta=0.4$, 0.6, 0.8, and 1.0, $\alpha_s=0.12$ and $C_R=4/3$.

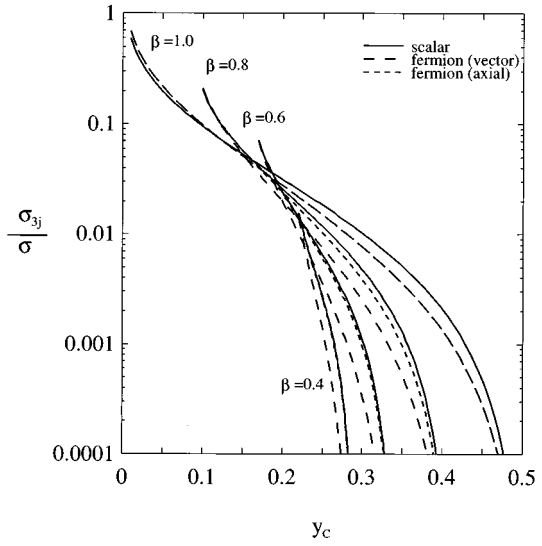

FIG. 7. Same as Fig. 6, but as a function of a jet-defining variable y_c.

where $y_g=(p+\overline{p})/s$. Since the region $y_g\to 0$ (or $y_g\to 4m^2/s$) contains no singularity, this definition does not lead to significant modification of the result for small y_c. In the high-energy limit $\beta\to 1$, the three-jet fraction is found to be

$$\sigma_{3j}/\sigma_0=\frac{C_R\alpha_s}{\pi}\left[2\mathrm{Li}_2\left(\frac{y_c}{1-y_c}\right)+\ln^2\frac{1-y_c}{y_c}-\frac{\pi^2}{6}-2(1-2y_c)\ln\frac{1-2y_c}{y_c}+3(1-y_c)(1-3y_c)\right], \tag{4.12}$$

whereas for fermions (both vector and axial) we have

$$\sigma_{3j}/\sigma_0=\frac{C_R\alpha_s}{\pi}\left[2\mathrm{Li}_2\left(\frac{y_c}{1-y_c}\right)+\ln^2\frac{1-y_c}{y_c}-\frac{\pi^2}{6}-\frac{3}{2}(1-2y_c)\ln\frac{1-2y_c}{y_c}+\tfrac{1}{4}(1-3y_c)(5+3y_c)\right]. \tag{4.13}$$

V. CONCLUSIONS

We have studied $O(\alpha_s)$ QCD correction to colored scalar pair production in e^+e^- annihilation. Emphasis is put on gluon emission in the final state. We compared the configuration of the three-jet final state with those in fermion pair production and found that the two cross sections are quantitatively quite different. This has to be taken into account in the search and study of production of scalar particles such as squarks and leptoquarks at the CERN e^+e^- collider LEP 2 and future linear colliders.

In calculating the helicity amplitudes $e^+e^-\to\zeta\overline{\zeta g}$, we found that it is convenient to decompose the amplitude into two subprocesses $e^+e^-\to V^*(V^*=\gamma,Z)$ and $V^*\to\zeta\overline{\zeta g}$. The amplitudes take a simple form if one works in two different Lorentz frames, the e^+e^- c.m. frame for the former and the $\zeta\overline{\zeta}$ c.m. frame in the latter. In particular, working in the ''quasi-two-body'' frame in the latter $1\to 3$ subprocess allows one to take advantage of the strong constraints of rotational invariance on two-body states.

ACKNOWLEDGMENTS

One of us (J. H.) thanks the Japan Society for the Promotion of Science for financial support. This work is partly supported by Grant-in-Aid for Scientific Research No. 06640369 from the Japan Ministry of Education, Science, Sports, and Culture.

APPENDIX A: HELICITY AMPLITUDES FOR $e^+e^-\to\zeta\overline{\zeta g}$

A number of formulations [9] for calculating helicity amplitudes [10] are found in the literature. Most of them are particularly suited for many-body final states and numerical evaluation of the amplitudes. The technique we employ here is a method [11] based on the spherical-vector basis, which is well-suited for manual analytic calculations and gives amplitudes with clear physical interpretations. The method is most useful for $2\to 2$ body processes (also $1\to 2$, $2\to 1$). In these processes, angular momentum conservation strongly constrains the form of the amplitudes. In our technique, this constraint can be explicitly extracted in the form of a Wigner D function that depends on the scattering angles. This part represents the variation of the amplitude that is imposed by kinematics. The rest of the amplitude contains purely dynamical information.

In general, the helicity amplitude for the process

$$a(p_a,\lambda_a)+b(p_b,\lambda_b)\to c(p_c,\lambda_c)+d(p_d,\lambda_d)$$

(λ_a is the helicity of the particle a, etc.) in the c.m. frame can be written as

$$\mathcal{M}=\tilde{\mathcal{M}}(E_{\mathrm{c.m.}},\cos\theta;\{\lambda\})d^{J_0}_{\lambda_i,\lambda_f}(\theta)e^{i(\lambda_i-\lambda_f)\phi}, \tag{A1}$$

where $\lambda_i=\lambda_a-\lambda_b$, $\lambda_f=\lambda_c-\lambda_d$, $J_0=\max(\lambda_i,\lambda_f)$, and (θ,ϕ) are the scattering angles [in the frame $\vec{p}_a$ is along the z axis, $\vec{p}_c$ is in the direction (θ,ϕ)]. The $d^J_{\lambda\lambda'}$ is the Wigner d function. The last two factors in this formula represent the ''minimal'' angular distribution imposed by the kinematics. The physical meaning of J_0 is the smallest allowed angular momentum for the process. The $\cos\theta$ dependence of $\tilde{\mathcal{M}}$ comes from higher partial waves with $J>J_0$. If the process has only one partial wave J (e.g., for two-body decays or $e^+e^-\to\mu^+\mu^-$), the whole angular dependence can be extracted in the form of d^J and the ϕ-dependent phase factor.

This technique can be applied to the process we consider if we note the following two points.

(1) The amplitude can be decomposed into two parts: (a) production of a virtual vector boson V^*, $e^+e^-\to V^*$ ($V=\gamma$ or Z); (b) the virtual vector boson decaying to $\zeta\overline{\zeta g}$. The helicity amplitude for the whole process is the product of the two amplitudes with a fixed V^* helicity ($\lambda_V=\pm 1,0$), which are then summed over:

$$\mathcal{M}=-\sum_V\frac{1}{s-m_V^2}\sum_{\lambda_V=\pm 1,0}\mathcal{M}(e^-e^+\to V^*)\times\mathcal{M}(V^*\to\zeta\overline{\zeta g}). \tag{A2}$$

[Note that we need three polarization states for both γ^* and Z^*. A fourth (scalar) polarization state need not be included since V^* couples to a conserved current.]

(2) The helicity amplitude for the second $1\to3$ process $V^*(q)\to\zeta(p)+\bar{\zeta}(\bar{p})+g(k)$ can be treated in the same way as $2\to2$ processes if one works in the ''quasi-two-body'' frame, the c.m. frame of *two* of the final particles (e.g., $\zeta\bar{\zeta}$), not in the V^* c.m. frame. This frame is related to the e^+e^- c.m. frame by a boost along the gluon direction.

First, we list the helicity amplitudes for $V^*(q,\lambda_V)\to\zeta(p)+\bar{\zeta}(\bar{p})+g(k,\lambda)$ (note that the scalar particles have zero helicities). We take the V^* (and g) direction as the z axis, and the ζ direction as (θ,ϕ). We follow the Jacob-Wick convention to fix the phase of the fermion-vector wave functions. The amplitudes can be written as

$$\mathcal{M}(V^*\to\zeta\bar{\zeta}g)=g_f g_s T^a\tilde{\mathcal{M}}, \tag{A3}$$

with

$$g_f=\begin{cases} Q_\zeta e & \text{for } V=\gamma, \\ e(T_{3\zeta}-Q_\zeta\sin^2\theta_W)/\sin\theta_W\cos\theta_W & \text{for } V=Z, \end{cases} \tag{A4}$$

and $\tilde{\mathcal{M}}$ given by

$\lambda_n\equiv\lambda_V-\lambda=\pm2$

$$\tilde{\mathcal{M}}=\frac{2\tau v^2\sin^2\theta}{(1-\tau)(1-v^2\cos^2\theta)}\,e^{i\lambda_n\phi}, \tag{A5}$$

$\lambda_n\equiv\lambda_V-\lambda=\pm1$

$$\tilde{\mathcal{M}}=\mp\frac{2\sqrt{2\tau}v^2\sin\theta\,\cos\theta}{(1-\tau)(1-v^2\cos^2\theta)}\,e^{i\lambda_n\phi}, \tag{A6}$$

$\lambda_n\equiv\lambda_V-\lambda=0$

$$\tilde{\mathcal{M}}=-\frac{2\tau v^2\sin^2\theta}{(1-\tau)(1-v^2\cos^2\theta)}-2. \tag{A7}$$

The helicity amplitude for $e^-e^+\to V^*$ is simpler. We take the V^* direction as the z axis and the e^- direction lying on the xz plane (with a positive x component). The angle between the two directions is denoted by Θ. This choice is made to relate the two frames by the boost along the z axis, under which the helicity of V^* does not change. The amplitude conserves electron chirality so that only $\lambda_i=\lambda(e^-)-\lambda(e^+)=\pm1$ is allowed:

$$\mathcal{M}=(-1)^{\lambda_V}g_i\sqrt{2s}\,d^1_{\lambda_i\lambda_V}(\Theta),$$

with

$$g_i=\begin{cases} -e & \text{for } V=\gamma,\quad \lambda_i=\pm1, \\ e(v_e\mp a_e)/\sin\theta_W\cos\theta_W & \text{for } V=Z,\quad \lambda_i=\pm1. \end{cases} \tag{A8}$$

The explicit form of the d functions needed is

$$d^1_{\lambda\mu}(\Theta)=\begin{cases} \frac{1}{2}(1+\lambda\mu\,\cos\Theta) & |\lambda|=|\mu|=1, \\ -\dfrac{\lambda}{\sqrt{2}}\sin\Theta & |\lambda|=1,\quad \mu=0 \end{cases}. \tag{A9}$$

APPENDIX B: THREE-BODY PHASE SPACE

The differential cross section can be calculated from the helicity amplitudes with the Lorentz-invariant three-body phase space

$$d\Phi_3=(2\pi)^4\delta^4(q-p-\bar{p}-k)\times\frac{d^3p}{(2\pi)^3 2p^0}\,\frac{d^3\bar{p}}{(2\pi)^3 2\bar{p}^0}\,\frac{d^3k}{(2\pi)^3 2k^0}, \tag{B1}$$

which in terms of the kinematic variables defined in Section III is

$$d\Phi_3=\frac{sv(1-\tau)}{1024\pi^4}\,d\tau\,d\cos\Theta\,d\cos\theta\,d\phi, \tag{B2}$$

where $1-\beta^2<\tau<1$, and $v=(1-4m^2/\tau s)^{1/2}$ is the ζ velocity in the $\zeta\bar{\zeta}$ c.m. frame. (We have integrated over one azimuthal angle on which the cross section has trivial dependence.)

Two of the kinematic variables, τ and θ, specify the final-state configuration and the other two determine the orientation of the configuration with respect to the initial beam axis. Integrating over Θ and ϕ one has

$$d\Phi_3=\frac{sv(1-\tau)}{256\pi^3}\,d\tau\,d\cos\theta. \tag{B3}$$

For analytic integration over the three-body phase space for $m\neq0$, it is easier to use $(\cos\theta,v)$ as the integration variables, for which the integration region is $0<v<\beta,-1<\cos\theta<1$:

$$d\Phi_3=\frac{s(1-\beta^2)}{128\pi^3}\,\frac{v^2(\beta^2-v^2)}{(1-v^2)^3}\,dv\,d\cos\theta. \tag{B4}$$

The variables $(x,\bar{x})$ have a special property for which the phase-space density is constant (Dalitz variables):

$$d\Phi_3=\frac{s}{128\pi^3}\,dx\,d\bar{x}. \tag{B5}$$

The translation is made using

$$\tau=1-x-\bar{x},\quad v\,\cos\theta=-\frac{x-\bar{x}}{x+\bar{x}}. \tag{B6}$$

The physical phase-space region is bounded by the inequality

$$x\bar{x}(1-x-\bar{x})-\frac{m^2}{s}\,(x+\bar{x})^2>0. \tag{B7}$$

APPENDIX C: FORMULAS FOR FERMION PAIR PRODUCTION

We collect results for the familiar process of fermion pair production $e^+e^-\to FF(g)$ [2,12,13] in this Appendix. These results have been independently calculated by us. The $FF\gamma$ and FFZ vertices in the lowest order have the form

$$-ieQ_F\gamma_\mu \quad \text{and} \quad -\frac{ie}{\cos\theta_W\sin\theta_W}\,\gamma_\mu(v_F-a_F\gamma_5), \tag{C1}$$

with

$$v_F=\tfrac{1}{2}[T_3(F_L)+T_3(F_R)]-Q_F\sin^2\theta_W, \tag{C2}$$

$$a_F=\tfrac{1}{2}[T_3(F_L)-T_3(F_R)]. \tag{C3}$$

At $O(\alpha_s)$, the correction factor is common for the photon and the vector part of the Z current. The axial part of the Z current is modified differently if $m_F\neq 0$. We write the general Lorentz structure of the vector and axial vertices for on-shell fermions,

$$\Gamma_\mu=F_1^V(q^2)\gamma_\mu+F_2^V(q^2)i\sigma_{\mu\nu}q^\nu/m_F \tag{C4}$$

for the vector current, and

$$\Gamma_\mu^5=F_1^A(q^2)\gamma_\mu\gamma_5+F_2^A(q^2)q_\mu\gamma_5/m_F \tag{C5}$$

for the axial vector current. We have retained only terms appearing at $O(\alpha_s)$, i.e., terms allowed by CP invariance and vector current conservation. We normalize the vertices such that $F_1^{V,A}=1$ at the lowest order. $F_2^{V,A}$ do not appear in this order.

We write the $O(\alpha_s)$ corrected vertices as

$$F_1^{V,A}(q^2)=1+\frac{C_R\alpha_s}{2\pi}\,f_1^{V,A}(q^2), \tag{C6}$$

$$F_2^{V,A}(q^2)=\frac{C_R\alpha_s}{2\pi}\,f_2^{V,A}\,(q^2). \tag{C7}$$

We find the renormalized vector form factors for $q^2>4m_F^2$:

$$\begin{aligned}f_1^V=&\left(-\frac{1+\beta^2}{2\beta}\ln\frac{1+\beta}{1-\beta}+1\right)\ln\frac{m_F^2}{\lambda^2}+\frac{1+\beta^2}{\beta}\left[\mathrm{Li}_2\left(\frac{1-\beta}{1+\beta}\right)\right.\\&\left.+\ln\frac{1+\beta}{2\beta}\ln\frac{1+\beta}{1-\beta}-\tfrac{1}{4}\ln^2\frac{1+\beta}{1-\beta}+\frac{\pi^2}{3}\right]\\&+\frac{1+2\beta^2}{2\beta}\ln\frac{1+\beta}{1-\beta}-2+i\pi\left[\frac{1+\beta^2}{2\beta}\left(\ln\frac{m_F^2}{\lambda^2}\right.\right.\\&\left.\left.+\ln\frac{4\beta^2}{1-\beta^2}\right)-\frac{1+2\beta^2}{2\beta}\right],\end{aligned} \tag{C8}$$

$$f_2^V=\frac{1-\beta^2}{4\beta}\left(-\ln\frac{1+\beta}{1-\beta}+i\pi\right), \tag{C9}$$

where $\beta=(1-4m_F^2/q^2)^{1/2}$. We have used on-mass-shell renormalization condition such that $F_1^V(0)=1$. Once the prescription for the vector vertex is fixed, there is no freedom to choose a renormalization condition for the axial vertex because of electroweak gauge symmetry. In particular, $F_1^A(0)$ *deviates* from unity. The axial form factors are found to be

$$\begin{aligned}f_1^A=&\left(-\frac{1+\beta^2}{2\beta}\ln\frac{1+\beta}{1-\beta}+1\right)\ln\frac{m_F^2}{\lambda^2}+\frac{1+\beta^2}{\beta}\left[\mathrm{Li}_2\left(\frac{1-\beta}{1+\beta}\right)\right.\\&\left.+\ln\frac{1+\beta}{2\beta}\ln\frac{1+\beta}{1-\beta}-\tfrac{1}{4}\ln^2\frac{1+\beta}{1-\beta}+\frac{\pi^2}{3}\right]\\&+\frac{2+\beta^2}{2\beta}\ln\frac{1+\beta}{1-\beta}-2+i\pi\left[\frac{1+\beta^2}{2\beta}\left(\ln\frac{m_F^2}{\lambda^2}+\ln\frac{4\beta^2}{1-\beta^2}\right)\right.\\&\left.-\frac{2+\beta^2}{2\beta}\right],\end{aligned} \tag{C10}$$

$$f_2^A=\frac{1-\beta^2}{4\beta}\left[(2+\beta^2)\left(-\ln\frac{1+\beta}{1-\beta}+i\pi\right)+2\beta\right]. \tag{C11}$$

The second form factor F_2^A represents the pseudoscalar part of the axial current and does not contribute to the reaction we are interested in as long as the electron mass is neglected.

The differential cross section for the three-body FFg final state is for the vector current

$$\begin{aligned}\frac{d\sigma_\pm^V}{d\tau\,d\,\cos\theta}=&\sigma_{0\pm}^V\,\frac{C_R\alpha_s}{\pi}\,\frac{v(1-\tau)}{\beta(3-\beta^2)}\left[\frac{1+v^2\cos^2\theta}{1-v^2\cos^2\theta}\right.\\&\left.+\frac{2(3-\beta^2)\tau v^2\sin^2\theta}{(1-\tau)^2(1-v^2\cos^2\theta)^2}\right],\end{aligned} \tag{C12}$$

and for the axial vector current

$$\begin{aligned}\frac{d\sigma_\pm^A}{d\tau\,d\,\cos\theta}=&\sigma_{0\pm}^A\,\frac{C_R\alpha_s}{\pi}\,\frac{v(1-\tau)}{2\beta^3}\left[\frac{2-\beta^2+v^2\cos^2\theta}{1-v^2\cos^2\theta}\right.\\&\left.+\frac{4\beta^2\tau v^2\sin^2\theta}{(1-\tau)^2(1-v^2\cos^2\theta)^2}\right],\end{aligned} \tag{C13}$$

with the lowest-order cross sections

$$\sigma_{0\pm}^V=\frac{8\pi d_R\alpha^2}{3s}\,H_{V\pm}^2\,\frac{\beta(3-\beta^2)}{2}, \tag{C14}$$

$$\sigma_{0\pm}^A=\frac{8\pi d_R\alpha^2}{3s}\,H_{A\pm}^2\beta^3. \tag{C15}$$

Here $H_{V\pm}$ and $H_{A\pm}$ are given by

$$H_{V\pm}=-Q_F+\frac{(v_e\mp a_e)v_F}{\cos^2\theta_W\sin^2\theta_W}\,\frac{s}{s-m_Z^2}, \tag{C16}$$

$$H_{A\pm}=\frac{(v_e\mp a_e)a_F}{\cos^2\theta_W\sin^2\theta_W}\,\frac{s}{s-m_Z^2}. \tag{C17}$$

In terms of the Dalitz variables, we have for the vector current

$$\frac{d\sigma_{\pm}^{V}}{dx\,d\bar{x}}=\sigma_{0\pm}^{V}\,\frac{C_R\alpha_s}{\pi}\,\frac{1}{\beta}\left[\frac{1}{3-\beta^2}\left(\frac{\bar{x}}{x}+\frac{x}{\bar{x}}\right)-\left(\frac{1}{x}+\frac{1}{\bar{x}}\right)+\frac{1+\beta^2}{2}\,\frac{1}{x\bar{x}}-\frac{1-\beta^2}{4}\left(\frac{1}{x^2}+\frac{1}{\bar{x}^2}\right)\right]. \tag{C18}$$

and for the axial vector current

$$\frac{d\sigma_{\pm}^{A}}{dx\,d\bar{x}}=\sigma_{0\pm}^{A}\,\frac{C_R\alpha_s}{\pi}\,\frac{1}{\beta}\left[\frac{3-\beta^2}{4\beta^2}\left(\frac{\bar{x}}{x}+\frac{x}{\bar{x}}\right)+\frac{1-\beta^2}{2\beta^2}-\left(\frac{1}{x}+\frac{1}{\bar{x}}\right)+\frac{1+\beta^2}{2}\,\frac{1}{x\bar{x}}-\frac{1-\beta^2}{4}\left(\frac{1}{x^2}+\frac{1}{\bar{x}^2}\right)\right]. \tag{C19}$$

The total $O(\alpha_s)$ correction can be written as the sum of the three contributions, virtual, soft, and hard corrections. We list each correction term for the scalar-pair production for comparison:

$$\Delta_{\text{virtual}}=\frac{1}{\beta}\,A_v(\beta)+\frac{1+\beta^2}{\beta}\,\ln\frac{1+\beta}{1-\beta}-2, \tag{C20}$$

$$\Delta_{\text{soft}}=\frac{1}{\beta}\,A_s(\beta)+\frac{1}{\beta}\,\ln\frac{1+\beta}{1-\beta}, \tag{C21}$$

$$\Delta_{\text{hard}}=\frac{1}{\beta}\,A_h(\beta)-\frac{1}{4\beta^3}\,(3+\beta^2)(1-\beta^2)\ln\frac{1+\beta}{1-\beta}+\frac{1}{2\beta^2}\,(3+7\beta^2), \tag{C22}$$

where we have collected the ''dilogarithmic'' part (dilogarithm and double log terms) into the functions $A_i(i=v,s,h)$:

$$A_v(\beta)=\left(-\frac{1+\beta^2}{2}\,\ln\frac{1+\beta}{1-\beta}+\beta\right)\ln\frac{m^2}{\lambda^2}+(1+\beta^2)\times\left[\mathrm{Li}_2\left(\frac{1-\beta}{1+\beta}\right)-\ln\frac{2\beta}{1+\beta}\,\ln\frac{1+\beta}{1-\beta}-\tfrac{1}{4}\,\ln^2\frac{1+\beta}{1-\beta}+\frac{\pi^2}{3}\right], \tag{C23}$$

$$A_s(\beta)=\left(\frac{1+\beta^2}{2}\,\ln\frac{1+\beta}{1-\beta}-\beta\right)\ln\frac{4\omega^2}{\lambda^2}+(1+\beta^2)\times\left[\mathrm{Li}_2\left(\frac{1-\beta}{1+\beta}\right)-\ln\frac{2\beta}{1+\beta}\,\ln\frac{1+\beta}{1-\beta}-\tfrac{1}{4}\,\ln^2\frac{1+\beta}{1-\beta}-\frac{\pi^2}{6}\right], \tag{C24}$$

$$A_h(\beta)=\left(\frac{1+\beta^2}{2}\,\ln\frac{1+\beta}{1-\beta}-\beta\right)\ln\frac{m^2}{4\omega^2}+(1+\beta^2)\times\left[2\,\mathrm{Li}_2\left(\frac{1-\beta}{1+\beta}\right)+2\,\mathrm{Li}_2\left(-\frac{1-\beta}{1+\beta}\right)-\ln\frac{2}{1+\beta}\,\ln\frac{1+\beta}{1-\beta}+\tfrac{1}{2}\,\ln^2\frac{1+\beta}{1-\beta}-\frac{\pi^2}{6}\right]-3\beta\,\ln\frac{4}{1-\beta^2}-4\beta\,\ln\beta. \tag{C25}$$

The function $A(\beta)$ in Eq. (3.17) is the sum of these three:

$$A(\beta)=A_v(\beta)+A_s(\beta)+A_h(\beta). \tag{C26}$$

Turning to the fermion-pair production, it is found that the dilogarithmic terms are exactly the same as for the scalar-pair production. For the vector part we find

$$\Delta_{\text{virtual}}^{V}=\mathrm{Re}\,f_1^V+\frac{6}{3-\beta^2}\,\mathrm{Re}\,f_2^V=\frac{1}{\beta}\,A_v(\beta)+\frac{\beta(4-\beta^2)}{3-\beta^2}\,\ln\frac{1+\beta}{1-\beta}-2, \tag{C27}$$

$$\Delta_{\text{soft}}^{V}=\frac{1}{\beta}\,A_s(\beta)+\frac{1}{\beta}\,\ln\frac{1+\beta}{1-\beta}, \tag{C28}$$

$$\Delta_{\text{hard}}^{V}=\frac{1}{\beta}\,A_h(\beta)+\frac{9-2\beta^2+\beta^4}{8\beta(3-\beta^2)}\,\ln\frac{1+\beta}{1-\beta}+\frac{39-17\beta^2}{4(3-\beta^2)}, \tag{C29}$$

and, for the axial vector part,

$$\Delta_{\text{virtual}}^{A}=\frac{1}{\beta}\,A_v(\beta)+\frac{2+\beta^2}{2\beta}\,\ln\frac{1+\beta}{1-\beta}-2, \tag{C30}$$

$$\Delta_{\text{soft}}^{A}=\frac{1}{\beta}\,A_s(\beta)+\frac{1}{\beta}\,\ln\frac{1+\beta}{1-\beta}, \tag{C31}$$

$$\Delta_{\text{hard}}^{A}=\frac{1}{\beta}\,A_h(\beta)+\frac{1}{32\beta^3}\,(21-5\beta^2+3\beta^4-3\beta^6)\ln\frac{1+\beta}{1-\beta}+\frac{1}{16\beta^2}\,(-21+62\beta^2+3\beta^4). \tag{C32}$$

[1] Particle Data Group, R. M. Barnett *et al.*, Phys. Rev. D **54**, 1 (1996).

[2] J. Schwinger, *Particles, Sources, and Fields*, Vol. II (Addison-Wesley, Reading, MA, 1973), Chap. 5-4.

[3] M. Drees and K. Hikasa, Phys. Lett. B **252**, 127 (1990).

[4] W. Beenakker, R. Höpker, and P. M. Zerwas, Phys. Lett. B **349**, 463 (1995).

[5] A. Arhrib, M. Capdequi-Peyranere, and A. Djouadi, Phys. Rev. D **52**, 1404 (1995).

[6] G. 't Hooft and M. Veltman, Nucl. Phys. **B153**, 365 (1979).

[7] I. I. Bigi, V. S. Fadin, and V. Khoze, Nucl. Phys. **B377**, 461 (1992).

[8] V. S. Fadin and V. A. Khoze, JETP Lett. **46**, 525 (1987); Sov. J. Nucl. Phys. **48**, 309 (1988); M. Strassler and M. Peskin, Phys. Rev. D **43**, 1500 (1991).

[9] See, e.g., P. de Causmaecker *et al.*, Nucl. Phys. **B206**, 53 (1982); Zh. Xu, D.-H. Zhang, and L. Chang, *ibid*. **B291**, 392 (1987); S. J. Parke and T. R. Taylor, Phys. Lett. **157B**, 81

(1985); **174**, 465(E) (1986); A. Kersch and F. Scheck, Nucl. Phys. **B263**, 475 (1986); J. F. Gunion and Z. Kunszt, Phys. Lett. **161B**, 333 (1985); R. Kleiss and W. J. Stirling, Nucl. Phys. **B262**, 235 (1985); K. Hagiwara and D. Zeppenfeld, Nucl. Phys. **B274**, 1 (1986); F. A. Berends and W. Giele, Nucl. Phys. **B294**, 700 (1987); V. Barger, J. Ohnemus, and R. J. N. Phillips, Phys. Rev. D **35**, 166 (1987).

[10] M. Jacob and G. C. Wick, Ann. Phys. (N.Y.) **7**, 404 (1959).

[11] K. Hikasa (unpublished).

[12] B. L. Ioffe, Phys. Lett. **78B**, 277 (1978); G. Grunberg, Y. J. Ng, and S.-H. H. Tye, Phys. Rev. D **21**, 62 (1980); **36**, 311(E) (1987).

[13] J. Jersák, E. Laermann, and P. M. Zerwas, Phys. Rev. D **25**, 1218 (1982); A. Djouadi, Z. Phys. C **39**, 561 (1988); J. G. Körner, A. Pilaftsis, and M. M. Tung, *ibid*. **63**, 575 (1994).